Affine-null formulation of the gravitational equations: Spherical case

J. A. Crespo,[1] H. P. de Oliveira,[1] and J. Winicour[2,3]

[1]*Departamento de Fisica Teorica, Instituto de Fisica, Universidade do Estado do Rio de Janeiro, CEP 20550-013. Rio de Janeiro, RJ, Brazil*

[2]*Department of Physics and Astronomy, University of Pittsburgh, Pittsburgh, Pennsylvania 15260, USA*

[3]*Max-Planck-Institut für Gravitationsphysik, Albert-Einstein-Institut, 14476 Golm, Germany*

(Received 9 October 2019; published 8 November 2019)

A new evolution algorithm for the characteristic initial value problem based upon an affine parameter rather than the areal radial coordinate used in the Bondi-Sachs formulation is applied in the spherically symmetric case to the gravitational collapse of a massless scalar field. The advantages over the Bondi-Sachs version are discussed, with particular emphasis on the application to critical collapse. Unexpected quadratures lead to a simple evolution algorithm based upon ordinary differential equations which can be integrated along the null rays. For collapse to a black hole in a Penrose compactified spacetime, these equations are regularized throughout the exterior and interior of the horizon up to the final singularity. They are implemented as a global numerical evolution code based upon the Galerkin method. New results regarding the global properties of critical collapse are presented.

DOI: 10.1103/PhysRevD.100.104017

I. INTRODUCTION

The Bondi-Sachs formulation of Einstein equations [1,2], in which the coordinates are adapted to the null geodesics of the spacetime, provided historic and convincing evidence that the emission of gravitational waves is accompanied by mass loss from the system. (For a review see [3].) A technical limitation in the application of the Bondi-Sachs formulation arises from the use of an areal radial coordinate to parametrize the outgoing null geodesics. The areal coordinate becomes singular on and inside the event horizon so that the Bondi-Sachs formalism is only applicable in the exterior of the horizon. An alternative approach [4] replaces the areal coordinate by an affine parameter.

The difference in behavior between an areal coordinate r and an affine parameter λ arises from focusing effects on the null rays. The affine coordinate λ only becomes singular at points where the null rays intersect, e.g., caustics, whereas the areal coordinate r also becomes singular at points where the expansion of the null rays vanish, i.e., where $\partial_\lambda r = 0$. The Bondi-Sachs formulation was originally adopted for developing the PITT null code [5,6] for simulating gravitational wave production because the hierarchical structure of its system of equations allows them to be integrated sequentially for one variable at a time along the outgoing null geodesics. This hierarchical structure greatly simplifies the evolution algorithm and is thought to underly its stability. An affine parameter coordinate was not adopted because this hierarchical integration structure was apparently broken. However, by introducing a (not so obvious) choice of variables, it was recently shown how the hierarchical structure of the affine-null system can be regained [4].

An early triumph of numerical relativity was Choptuik's discovery of critical phenomena in the spherically symmetric gravitational collapse of a massless scalar wave [7]. Critical collapse marks the threshold between a system collapsing to form a black hole or expanding to form an asymptotically Minkowskian state. The use of an areal coordinate for studying critical collapse is an impediment because of its singular nature at the event horizon. In the Bondi-Sachs treatment of spherically symmetric gravitational collapse this is not so serious because the event horizon forms at a single retarded time, i.e., simultaneously in all radial null directions from the center of symmetry. However, the ability to penetrate the event horizon, as by the affine-null system, is critical in attacking the non-symmetric case, where the event horizon forms at different retarded times for different angles. Some initial results have been obtained for the critical collapse of axisymmetric gravitational waves [8,9] but fundamental questions remain that have relevance for cosmic censorship and quantum gravity. See [10,11] for reviews and discussions of how the critical solution acts as an attractor for this problem. The affine-null system offers promising potential for attacking this problem. As a first attempt in this direction we apply it here to the spherically symmetric Choptuik problem. A spherically symmetric affine-null system has also been applied in cosmology [12] and recently to the double null characteristic initial value problem [13].

Most numerical studies of critical collapse have used Cauchy evolution codes, with collapse to a black hole monitored by the formation of an apparent horizon. A notable exception by Pürrer *et al.* [14] treats the spherically

symmetric Choptuik problem by means of the Bondi-Sachs formulation. Their use of a compactified grid including future null infinity $\mathcal{I}^+$ allowed them to study how the Bondi mass and other features of asymptotic flatness behave on approach to the critical solution, which is not asymptotically flat. Using mesh refinement, they confirmed the formation of the discrete self-similarity on approach to the critical state and resolved the fine structure in the universal scaling law for the mass. Their investigation using the Bondi-Sachs formalism was limited to the spacetime exterior to black hole formation. Other studies of the Choptuik problem using characteristic evolution codes based upon double null coordinates were confined to portions of the spacetime which did not include a compactification of $\mathcal{I}^+$ [15–17]. The afffine-null approach which we utilize here is applicable to the entire exterior spacetime extending to (compactified) $\mathcal{I}^+$ and to the interior of the black hole extending to the final singularity.

For the spherical symmetric Choptuik problem with gravity coupled to a massless field Φ, the affine-null system has intriguing features. The procedure for organizing the evolution system into hierarchical form allows two unexpected quadratures which lead to a simple evolution algorithm based upon ordinary differential equations which can be integrated along the outgoing null rays. The details of an evolution algorithm valid in the exterior of the event horizon are described in Sec. II. Then, in Sec. III, we introduce renormalized variables which lead to a well-behaved evolution algorithm for the entire spacetime extending from the initial null hypersurface to the final singularity.

Our study involves unresolved global aspects of the Choptuik problem, such as the question whether there is a Bondi mass gap and the effect of a nonzero Newman-Penrose constant [18] for the scalar field. The theory underlying these issues is discussed in Sec. IV.

The affine-null evolution algorithm is implemented as a numerical evolution code based upon the Galerkin method. Domain decomposition techniques are developed to enhance resolution. The numerical methods are described in Sec. V. New numerical results regarding critical collapse are presented in Sec. VI.

II. SPHERICAL SYMMETRY: BASIC EQUATIONS

The affine-null system [4] is based upon a family of outgoing null hypersurfaces $u = \text{const}$ with angular coordinates x^A labeling the null rays and an affine parameter λ to coordinate points along the rays. Here we consider the spherically symmetric case based upon the null hypersurfaces emanating from the central worldline $\mathcal{W}$, with regularity conditions at the vertex. In affine-null spherical coordinates $x^a = (u, \lambda, x^A)$, $x^A = (\theta, \phi)$, the line element takes the form

$$g_{ab}dx^a dx^b = -\mathcal{V}du^2 - 2dud\lambda + r^2(d\theta^2 + \sin^2\theta d\phi^2) \quad (1)$$

where the metric functions $(\mathcal{V}, r)$ depend upon u and λ and r is the areal radius of the null cones. Here the affine freedom $\lambda \to A(u, x^A)\lambda + B(u, x^A)$ has been used to prescribe the normalization $(\nabla^a u)\nabla_a \lambda = -1$ and to set $\lambda = 0$ on $\mathcal{W}$.

In order to investigate event horizon formation, we introduce coupling to a massless scalar field in the form

$$R_{ab} = \Phi_{,a}\Phi_{,b}, \quad (2)$$

where R_{ab} is the Ricci tensor. (We use the shorthand notation $\partial_a F = F_{,a}$ for derivatives.)

In spherical symmetry, a complete system of equations for the affine-null system [4] then reduces to

$$r_{,\lambda\lambda} = -\frac{r}{2}\Phi_{,\lambda}\Phi_{,\lambda}, \quad (3)$$

$$(\mathcal{V}rr_{,\lambda})_{,\lambda} = 1 + 2(r^2)_{,\lambda u} \quad (4)$$

and the scalar wave equation $\Box_g \Phi = 0$, which takes the form

$$(r^2\Phi_{,u})_{,\lambda} + (r^2\Phi_{,\lambda})_{,u} - (r^2\mathcal{V}\Phi_{,\lambda})_{,\lambda} = 0. \quad (5)$$

Following the procedure in [4], we introduce the variables

$$\rho \equiv r_{,u}, \quad (6)$$

$$\mathcal{Y} \equiv \mathcal{V} - 2\frac{\rho}{r_{,\lambda}}, \quad (7)$$

$$K \equiv 2(r_{,\lambda}\Phi_{,u} - \rho\Phi_{,\lambda}). \quad (8)$$

Then (3)–(5) take the hierarchical form

$$r_{,\lambda\lambda} = -\frac{r}{2}\Phi_{,\lambda}\Phi_{,\lambda}, \quad (9)$$

$$(\mathcal{Y}(r^2)_{,\lambda})_{,\lambda} = 2, \quad (10)$$

$$r\left(\frac{rK}{r_{,\lambda}}\right)_{,\lambda} - (r^2\mathcal{Y}\Phi_{,\lambda})_{,\lambda} = 0. \quad (11)$$

Given $\Phi(u, \lambda)$, these equations can be integrated sequentially to determine r, $\mathcal{Y}$, and K, in that order.

An evolution algorithm valid in the exterior of the horizon can be formulated by taking the u-derivative of (9),

$$\rho_{,\lambda\lambda} = -\frac{1}{2}\rho\Phi_{,\lambda}\Phi_{,\lambda} - r\Phi_{,\lambda}\Phi_{,u\lambda}, \quad (12)$$

which can be expressed in the form

$$\left(\frac{\rho}{r_{,\lambda}}\right)_{,\lambda\lambda} = -\frac{r\Phi_{,\lambda}}{2r_{,\lambda}}\left(\frac{K}{r_{,\lambda}}\right)_{,\lambda}. \tag{13}$$

Equations (9)–(11) and (13) are regular in the exterior of the event horizon where $r_{,\lambda} > 0$. They gives rise to the following evolution algorithm. Specify the initial data

$$\Phi(0,\lambda), \qquad u = 0, \qquad \lambda \geq 0 \tag{14}$$

and impose the regularity conditions at the central geodesic

$$\begin{aligned} r = 0, \qquad r_{,\lambda} = 1, \qquad \mathcal{Y} = 1, \\ rK = \rho = \rho_{,\lambda} = 0, \qquad u \geq 0, \qquad \lambda = 0. \end{aligned} \tag{15}$$

Using this initial data, integrate (9)–(11) and (13) in sequential order to determine the initial values of the variables $(r, \mathcal{Y}, K, \rho)$. Given this initialization and the vertex regularity conditions, the system can then be evolved to $u = \Delta u$ by a finite difference approximation to determine $r(\Delta u, \lambda)$ algebraically from ρ and to determine $\Phi(\Delta u, \lambda)$ algebraically from K. Then (10), (11) and (13) can be integrated in sequential order to determine $\mathcal{Y}$, K, and ρ at $u = \Delta u$. Repetition of this process provides the evolution algorithm.

In fact, this procedure can be simplified since (10) integrates to give

$$\mathcal{Y} = \frac{\lambda}{rr_{,\lambda}} \tag{16}$$

so that $\mathcal{Y}$ can be eliminated and (11) reduces to

$$\left(\frac{rK}{r_{,\lambda}}\right)_{,\lambda} = \frac{1}{r}\left(\frac{\lambda r\Phi_{,\lambda}}{r_{,\lambda}}\right)_{,\lambda}. \tag{17}$$

In the exterior of the event horizon, we assume that the initial data $\Phi(u_0, \lambda)$ has an asymptotic $1/\lambda$ expansion $\Phi(u_0, \lambda) = \alpha(u_0)\lambda^{-1} + \beta(u_0)\lambda^{-2} + \cdots$ so that it is consistent with asymptotic flatness. This asymptotic behavior is preserved in the exterior spacetime by the evolution equations, i.e.,

$$\Phi(u,\lambda) = \alpha(u)\lambda^{-1} + \beta(u)\lambda^{-2} + O(\lambda^{-3}). \tag{18}$$

Integration of (9) then leads to the asymptotic expansion

$$r = H(u)\lambda + R(u) - \frac{H\alpha^2}{4\lambda} + O(\lambda^{-2}). \tag{19}$$

III. REGULARIZED EVOLUTION INSIDE THE HORIZON

The expansion of the outgoing null cones is $\Theta^+ = 2r_{,\lambda}/r$. The regularity conditions at the vertex (15) require $r|_{\lambda=0} = 0$ and $r_{,\lambda}|_{\lambda=0} = 1$. Integration of (9) then implies $r_{,\lambda}$ decreases monotonically with λ, with the behavior near the vertex

$$r = \lambda - \frac{\lambda^3}{12}(\Phi_{,\lambda}(u,0))^2 + O(\lambda^4). \tag{20}$$

The radially inward pointing null vector is

$$n^a\partial_a = \partial_u - \frac{\mathcal{V}}{2}\partial_\lambda = \partial_u - \frac{(\lambda + 2r\rho)}{2rr_{,\lambda}}\partial_\lambda, \tag{21}$$

normalized by $n^a\partial_a u = 1$. The expansion of the ingoing null cones is

$$\Theta^- = \frac{4}{r}n^a\partial_a r = -\frac{2\lambda}{r^2}, \tag{22}$$

which is everywhere negative.

In the exterior untrapped region where $\Theta^+ > 0$, $H(u) = r_{,\lambda}|_{\lambda=\infty}$ satisfies $1 \geq H(u) > 0$, with equality $H = 1$ only in the trivial case $\Phi(u, r) = \text{const}$. In the supercritical case, on approach to the event horizon at $u = u_E$,

$$\lim_{u\to u_E} H(u) = 0. \tag{23}$$

Inside the event horizon there is an apparent horizon traced out by $\lambda = \lambda_A(u)$, where $r_{,\lambda}(u, \lambda_A) = 0$. After formation of the apparent horizon, the outgoing null cones from the central worldline recollapse to a singularity at $r = 0$ at a finite value of λ. Consequently, terms in the evolution equations (13) and (17) containing $1/r_{,\lambda}$ become singular at the apparent horizon. This is not a true singularity and there is a way to regularize the evolution system.

In order to regularize (17), we set

$$L = \frac{rK - \lambda\Phi_{,\lambda}}{r_{,\lambda}} = 2r\Phi_{,u} - \frac{(2r\rho + \lambda)\Phi_{,\lambda}}{r_{,\lambda}}. \tag{24}$$

As a result, (17) becomes

$$L_{,\lambda} = \frac{\lambda\Phi_{,\lambda}}{r}. \tag{25}$$

The right-hand side of (25) is regular everywhere in the exterior spacetime, including $\mathcal{I}^+$, and everywhere regular inside the event horizon up to the final singularity. Thus, as a result of the integration of (25), L is also regular everywhere.

In order to regularize the ρ equation (13) we introduce the variable

$$P = \frac{2r\rho + \lambda}{rr_{,\lambda}}. \tag{26}$$

Then, after considerable algebra involving the use of (25), we rewrite (13) as

$$P_{,\lambda\lambda} = \frac{2\lambda r_{,\lambda}}{r^3} - \frac{2}{r^2} + \frac{(L^2)_{,\lambda}}{2\lambda}. \tag{27}$$

The validity of (27) can be checked by straightforward calculation.

The right-hand side of (27) is regular everywhere in the spacetime up to the final singularity. Thus as a result of the integration of (27), using the vertex regularity conditions (15), P is also regular throughout the spacetime.

It is remarkable that (27) has a first integral. Multiplication by λ and use of the vertex regularity conditions, which require $P(u,0) = 1$ and $L(u,0) = 0$, leads after integration to

$$\left(\frac{P}{\lambda}\right)_{,\lambda} = -\frac{1}{r^2} + \frac{L^2}{2\lambda^2}. \tag{28}$$

Since P/λ is singular at the vertex, we introduce the variable

$$Q = (P-1)/\lambda = \frac{2r\rho + \lambda - r r_{,\lambda}}{\lambda r r_{,\lambda}}. \tag{29}$$

Then (28) becomes

$$Q_{,\lambda} = \frac{1}{\lambda^2} - \frac{1}{r^2} + \frac{L^2}{2\lambda^2}. \tag{30}$$

In summary, (3), (25) and (30) lead to the evolution system consisting of the three hypersurface equations

$$r_{,\lambda\lambda} = -\frac{r}{2}(\Phi_{,\lambda})^2, \tag{31}$$

$$L_{,\lambda} = \frac{\lambda \Phi_{,\lambda}}{r}, \tag{32}$$

$$Q_{,\lambda} = \frac{1}{\lambda^2} - \frac{1}{r^2} + \frac{L^2}{2\lambda^2}, \tag{33}$$

where the definitions of L and Q, (24) and (29), combine to give the evolution equation

$$\Phi_{,u} = \frac{\lambda Q}{2}\Phi_{,\lambda} + \frac{1}{2}\Phi_{,\lambda} + \frac{L}{2r}. \tag{34}$$

The ordinary differential equations (31)–(33) can be integrated along the outgoing null rays. The resulting solution is regular at the vertex, where $Q(u,0) = 0$ and $L(u,0) = 0$, is regular at $\mathcal{I}^+$, and is regular inside the horizon up to the final singularity. The system gives rise to the following evolution algorithm which covers the entire spacetime to the future of the initial null hypersurface. Given the initial data $\Phi(u_0,\lambda)$, integrate (31) to determine the initial value $r(u_0,\lambda)$. Then (32) and (33) can be integrated in sequential order to determine $L(u_0,\lambda)$, and $Q(u_0,\lambda)$. With these values $\Phi_{,u}(u_0,\lambda)$ is readily obtained from (34). Thus a finite difference approximation determines $\Phi(u_0 + \Delta u, \lambda)$. The repetition of this process provides a global evolution algorithm, whose numerical implementation is described in Sec. V. We integrate the resulting dynamical system using the Cash-Karp [19] method with an adaptive step size, where the initial step size is 10^{-4}.

Note that in the linearized limit, i.e., up to terms linear in Φ, (32) reduces to the flat space, spherically symmetric scalar wave equation and (33) implies $Q = 0$.

IV. PHYSICAL PROPERTIES

Bondi time u_B, i.e., the time intrinsic to an inertial observer at null infinity, is related to the central proper time by $\partial u_B/\partial u = 1/H$, where $H(u) = r_{,\lambda}(u,\lambda)|_{\lambda=\infty}$. In the supercritical case of event horizon formation at $u = u_E$, $H(u) \to 0$ as $u \to u_E$. Thus, although the horizon forms at a finite central time it forms at an infinite Bondi time, $u_B \to \infty$, in accord with the infinite redshift of a distant observer.

A. No scalar hair

The regularity of the affine-null evolution system implies that quantities that have finite u-derivatives on the event horizon, e.g., $\Phi_{,u}(u_E,\lambda)$, must have vanishing Bondi-time derivative so that $\partial_{u_B}\Phi(u_B,\lambda) \to 0$ as $u_B \to \infty$. This is consistent with the results of Christodoulou [20] obtained by applying the methods of analysis to the Bondi formulation of the Einstein-scalar equations. The scalar monopole moment is defined by

$$A(u) := \lim_{r\to\infty} r\Phi \tag{35}$$

so, referring to the asymptotic expansions (18) of Φ and (19) of r,

$$A(u) = \lim_{\lambda\to\infty} H\lambda\Phi = H(u)\alpha(u). \tag{36}$$

Of special importance, since $H(u_E) = 0$, it follows that $A(u) \to 0$ as $u \to u_E$, i.e., as $u_B \to \infty$, in accordance with the "no hair" property of the black hole.

B. Newman-Penrose constant

In Bondi coordinates, Φ has the asymptotic expansion

$$\Phi = \frac{A}{r} + \frac{c_{NP}}{r^2} + O(r^{-2})$$

where c_{NP} is the Newman-Penrose constant [18] for the scalar field. In order to express c_{NP} in affine-null coordinates we write

$$c_{NP} = -r^2\partial_r(r\Phi)|_{r=\infty} = -\frac{r^2}{r_{,\lambda}}\partial_\lambda(r\Phi)\Big|_{r=\infty}.$$

Then, from the asymptotic expansions (18) of Φ and (19) of r, we obtain

$$c_{NP} = H(\beta H + \alpha R). \tag{37}$$

In order to verify that $\partial_u c_{NP} = 0$ we consider the asymptotic expansion of the evolution equation (32) for L. From (24), we have

$$L = 2(H\alpha)_{,u} + \frac{1}{H\lambda}(2(RH\alpha + H^2\beta)_{,u} + \alpha) + \cdots. \tag{38}$$

But (32) implies

$$L_{,\lambda} = -\frac{\alpha}{H\lambda^2} + \left(\frac{R\alpha}{H} - 2\beta\right)\frac{1}{H\lambda^3} + \cdots. \tag{39}$$

Comparison of (38) with (39) gives $(RH\alpha + H^2\beta)_{,u} = 0$, in agreement with the conservation law $\partial_u c_{NP} = 0$.

As a result, the expansion (38) reduces to

$$L = 2(H\alpha)_{,u} + \frac{\alpha}{H\lambda} + \cdots, \tag{40}$$

and, to the next order,

$$L = 2(H\alpha)_{,u} + \frac{\alpha}{H\lambda} - \left(\frac{R\alpha}{H} - 2\beta\right)\frac{1}{2H\lambda^2} + \cdots. \tag{41}$$

In the numerical simulations we consider initial data of the form

$$\Phi(0,\lambda) = \frac{\epsilon}{a^2 + \lambda^2}, \tag{42}$$

for which $\alpha|_{u=0} = 0$ and $c_{NP} = \epsilon H^2|_{u=0}$ is a nonzero Newman-Penrose constant. This evolves to form a black hole for sufficiently large ϵ. The numerical behavior of the Newman-Penrose constant for slightly subcritical and slightly supercritical initial data is plotted in Sec. VI.

It might at first seem paradoxical that the Newman-Penrose constant must be conserved in the subcritical case where the scalar field vanishes, i.e., $\Phi \to 0$, as $u \to \infty$. This is explained by the nonuniform behavior of the limits $u \to \infty$ and $\lambda \to \infty$, which cannot be interchanged. As an example, consider Minkowski space where $\lambda = r$ and nonsingular solutions of the wave equation take the form

$$\Phi = \frac{f(t+r) - f(t-r)}{r} = \frac{f(u+2r) - f(u)}{r},$$

where f is a smooth function. Then the initial data (42) correspond to the flat space solution

$$\Phi = \frac{2\epsilon}{r}\left(\frac{u+2r}{a^2 + (u+2r)^2} - \frac{u}{a^2+u^2}\right)$$

with limit

$$\lim_{u\to\infty}\Phi = 0,$$

so that the scalar field decays to zero but

$$c_{NP} = -\lim_{r\to\infty} r^2\partial_r(r\Phi) = \epsilon,$$

independent of u.

C. The Bondi mass

In spherical symmetry the Misner-Sharp mass function $m(u,\lambda)$ is defined as [21]

$$1 - \frac{2m}{r} = g^{\alpha\beta}r_{,\alpha}r_{,\beta}. \tag{43}$$

In affine-null coordinates $g^{\alpha\beta}r_{,\alpha}r_{,\beta} = (\mathcal{V}r_{,\lambda} - 2\rho)r_{,\lambda} = \mathcal{Y}(r_{,\lambda})^2 = \lambda r_{,\lambda}/r$, where we have used (7) and (16). Therefore,

$$m(u,\lambda) = \frac{1}{2}(r - \lambda r_{,\lambda}). \tag{44}$$

The Bondi mass of the system is determined by taking the asymptotic limit

$$M_B(u) = \lim_{\lambda\to\infty} m(u,\lambda) = \frac{R(u)}{2}, \tag{45}$$

where $R(u)$ is obtained from the asymptotic expansion of r according to (19).

In order to recover the mass loss equation due to scalar radiation we consider the asymptotic behavior of the evolution equation for Q. From the definition (29) of Q and the asymptotic expansions (19) and (18), we obtain

$$Q = \frac{2H_{,u}}{H} + \frac{1 - H^2 + 2HR_{,u}}{H^2\lambda} + \cdots. \tag{46}$$

Using (40), the evolution equation (33) gives

$$Q_{,\lambda} = \frac{H^2 - 1 + 2[(HH\alpha)_{,u}]^2}{H^2\lambda^2} + \cdots. \tag{47}$$

Comparison with (46) gives the mass loss equation

$$M_{B,u} = \frac{1}{2}R_{,u} = -\frac{1}{2}H[(H\alpha)_{,u}]^2. \tag{48}$$

In the supercritical case, it follows that

$$\lim_{u\to u_E} M_{B,u} = \frac{1}{2}\lim_{u\to u_E} R_{,u} = 0 \tag{49}$$

on approach to the event horizon. The mass loss equation (48) provides a convenient test of code accuracy, as presented in Sec. VI.

D. Approach to horizon formation

Nontrivial data $\Phi(u_0,\lambda)$ implies $0 \le H(u_0) < 1$. In general, $H_{,u}$ can either be positive or negative. In the subcritical case in the limit that the spacetime becomes flat $H(u=\infty,\lambda)=1$, so that $H_{,u}>0$ at late times.

In the supercritical case, in the limit of horizon formation $H(u_E)=0$ so that $H_{,u}(u_E)\le 0$. As a result, the Bondi mass loss equation (48) leads to $M_{B,u}(u_E)=0$ and

$$M_{B,uu}(u_E) = -\frac{(H_{,u})^3}{2}\alpha^2|_{u=u_E} \ge 0.$$

Unless either $H_{,u}(u_E)=0$ or $\alpha(u_E)=0$, the inequality $M_{B,uu}(u_E)>0$ would hold in the limit so that $M_B(u_E)$ is a strong minimum. The numerical results in Sec. VI indicate that $H_{,u}(u_E)\ll 0$, i.e., that $H(u)$ goes to zero at a fast rate. But, generic numerical results show that $H_{,u}(u_E)\neq 0$ and $\alpha(u_E)\neq 0$, so that, $M_B(u_E)$ is a strong minimum.

Bondi time u_B at null infinity is related to the central proper time by $\partial u_B/\partial u = 1/H$. As a result, since $H_{,u}(u_E)$ is negative, on approach to the event horizon, $H(u)\sim H_{,u}(u_E)(u-u_E)$ and Bondi time goes to infinity as

$$u_B \sim \frac{\ln(u_E-u)}{H_{,u}(u_E)}. \tag{50}$$

V. NUMERICAL METHOD: THE GALERKIN-COLLOCATION APPROACH

To integrate the field equations, we have implemented a code based on the Galerkin-collocation method [22] using the domain decomposition technique. In general, single domain spectral methods are very accurate, but if we are to determine the formation of black holes of infinitesimal masses, it is necessary to establish a spectral version of mesh refinement provided by dividing the spatial domain into several subdomains.

We have implemented a simple version of the domain decomposition technique dividing the spatial domain $0\le\lambda<\infty$ into two noninterpolating subdomains, $\mathcal{D}_1: 0\le\lambda\le\lambda_0$ and $\mathcal{D}_2: \lambda_0\le\lambda<\infty$, where $\lambda=\lambda_0$ denotes the interface of these subdomains. The innovative part of implementing the algorithm is the two-step introduction of the correspondent computational, as indicated in Fig. 1. In the first step, the physical domain is compactified using the algebraic map [23]

$$\lambda = L_0\frac{(1+x)}{1-x}, \tag{51}$$

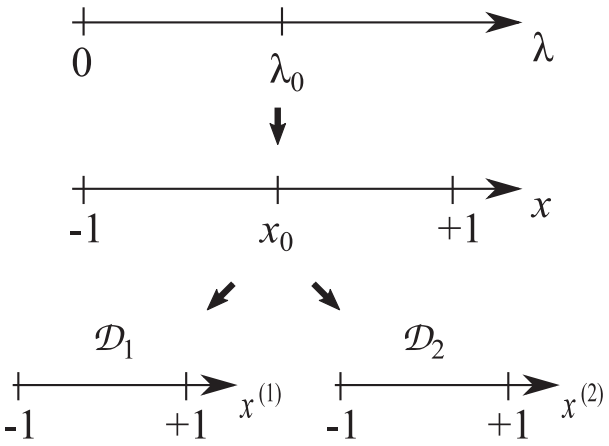

FIG. 1. Scheme showing the subdomains $\mathcal{D}_1$, $0\le\lambda\le\lambda_0$, and $\mathcal{D}_2$, $\lambda_0\le\lambda<\infty$. We also present the corresponding computational domains $-1\le x^{(A)}\le 1$ with $A=1,2$ for each domain.

so that the interval $0\le\lambda<\infty$ corresponds to $-1\le x\le 1$, and L_0 is the map parameter. In the second step, the subdomains $-1\le x\le x_0$ and $x_0\le x\le 1$ are mapped into the subdomains characterized by $-1\le x^{(1)}\le 1$ and $-1\le x^{(2)}\le 1$, respectively, by linear maps. For simplicity we have set the location of the interface at $x=x_0=0$ in the intermediate computational domain, which is equivalent to setting $\lambda_0=L_0$.

We approximate the relevant fields Φ, r, L, and Q as series with respect to appropriate sets of basis functions. According to the Galerkin method, each element of the basis functions must satisfy the boundary conditions of each subdomain. The approximations are shown in Table I. In these expressions N_A, $A=1,2$, are the truncation orders at each subdomain that dictate the number of unknown modes $a_k^{(A)}(u)$, $b_k^{(A)}(u)$, $c_k^{(A)}(u)$, $f_k^{(A)}(u)$. The basis functions $TL_k^{(A)}(\lambda)$ are the rational Chebyshev polynomials defined at each subdomain by

$$TL_k^{(1)}(\lambda) = T_k\left(x^{(1)}=\frac{3\lambda-L_0}{\lambda+L_0}\right), \tag{52}$$

$$TL_k^{(2)}(\lambda) = T_k\left(x^{(2)}=\frac{\lambda-3L_0}{\lambda+L_0}\right), \tag{53}$$

where $T_k(x)$ represents the standard Chebyshev polynomials of order k. The basis functions $\chi_k^{(1)}(\lambda)$ and $\psi_k^{(2)}(\lambda)$ are expressed in terms of the rational Chebyshev polynomials to satisfy the boundary conditions (cf. Table I). The domain decomposition method requires junction or transmission conditions for the relevant fields at the interface $\lambda=\lambda_0$. These conditions differ for the hypersurface and evolution equations. Starting with the hypersurface equations for L and P, we have

TABLE I. Spectral approximations of the scalar field and the metric functions $r^{(A)}(u,\lambda)$, $L^{(A)}(u,\lambda)$ and $Q^{(A)}(u,\lambda)$ in both subdomains together with the corresponding basis functions.

$\mathcal{D}_1: 0 \le \lambda \le \lambda_0$	$\mathcal{D}_2: \lambda_0 \le \lambda < \infty$
$\Phi^{(1)}(u,\lambda) = \sum_{k=0}^{N_1} a_k^{(1)}(u) TL_k^{(1)}(\lambda)$	$\Phi^{(2)}(u,\lambda) = \sum_{k=0}^{N_2} a_k^{(2)}(u) \psi_k^{(2)}(\lambda)$
$r^{(1)}(u,\lambda) = \lambda + \sum_{k=0}^{N_1} b_k^{(1)}(u) \lambda^3 TL_k^{(1)}(\lambda)$	$r^{(2)}(u,\lambda) = \sum_{k=0}^{N_2+2} b_k^{(2)}(u) \lambda TL_k^{(2)}(\lambda)$
$L^{(1)}(u,\lambda) = \sum_{k=0}^{N_1} c_k^{(1)}(u) \chi_k^{(1)}(\lambda)$	$L^{(2)}(u,\lambda) = \sum_{k=0}^{N_2+1} c_k^{(2)}(u) TL_k^{(2)}(\lambda)$
$Q^{(1)}(u,\lambda) = \sum_{k=0}^{N_1} f_k^{(1)}(u) \chi_k^{(1)}(\lambda)$	$Q^{(2)}(u,\lambda) = \sum_{k=0}^{N_2+1} f_k^{(2)}(u) TL_k^{(2)}(\lambda)$
Radial basis function:	Radial basis function:
$\chi_k^{(1)}(\lambda) = \frac{1}{2}(TL_{k+1}^{(1)}(\lambda) + TL_k^{(1)}(\lambda))$	$\psi_k^{(2)}(\lambda) = \frac{1}{2}(TL_{k+1}^{(2)}(\lambda) - TL_k^{(2)}(\lambda))$

$$L^{(1)}(u,\lambda_0) = L^{(2)}(u,\lambda_0), \quad \left(\frac{\partial L^{(1)}}{\partial u}\right)_{\lambda_0} = \left(\frac{\partial L^{(2)}}{\partial u}\right)_{\lambda_0}, \tag{54}$$

$$Q^{(1)}(u,\lambda_0) = Q^{(2)}(u,\lambda_0), \quad \left(\frac{\partial Q^{(1)}}{\partial u}\right)_{\lambda_0} = \left(\frac{\partial Q^{(2)}}{\partial u}\right)_{\lambda_0}. \tag{55}$$

The particular form of the hypersurface equation for the metric function $r(u,\lambda)$ demands the conditions

$$r^{(1)}(u,\lambda_0) = r^{(2)}(u,\lambda_0), \quad \left(\frac{\partial r^{(1)}}{\partial u}\right)_{\lambda_0} = \left(\frac{\partial r^{(2)}}{\partial u}\right)_{\lambda_0}, \tag{56}$$

$$\left(\frac{\partial^2 r^{(1)}}{\partial u^2}\right)_{\lambda_0} = \left(\frac{\partial^2 r^{(2)}}{\partial u^2}\right)_{\lambda_0}. \tag{57}$$

For the scalar field, it is necessary to guarantee its continuity at the interface,

$$\Phi^{(1)}(u,\lambda_0) = \Phi^{(2)}(u,\lambda_0). \tag{58}$$

Following Canuto *et al.* [24], we have adopted the average procedure where both subdomains have the same weight in the update equation for the interface point. This interface condition is

$$(\Phi_{,u})_{\lambda_0} - \frac{1}{2}\left[\frac{L^{(1)}}{2r^{(1)}} + \frac{1}{2}(1+\lambda Q^{(1)})\Phi^{(1)}_{,\lambda}\right]_{\lambda_0} - \frac{1}{2}\left[\frac{L^{(2)}}{2r^{(2)}} + \frac{1}{2}(1+\lambda Q^{(2)})\Phi^{(2)}_{,\lambda}\right]_{\lambda_0} = 0. \tag{59}$$

The final step in establishing the algorithm is to substitute the approximations of Table I into the field equations to form the residual equations in each subdomain. We have followed the collocation method by imposing that the residual equations vanish at the N_1 and N_2+1 interior collocation points in the subdomains $\mathcal{D}_1$ and $\mathcal{D}_2$, respectively. Therefore, there are N_1+N_2+1 equations that together with the transmission conditions provide the same number of unknown coefficients. For the sake of illustration, consider the residual equation associated to $r(u,\lambda)$ at the second domain,

$$\mathrm{Res}_{r^{(2)}}(u,\lambda_j) = \sum_{k=0}^{N_2+2} b_k^{(2)}[(\lambda TL_k^{(2)})_{,\lambda\lambda}]_j + \frac{1}{2} r_j^{(2)} (\Phi^{(2)}_{,\lambda})_j^2, \tag{60}$$

for all $j = 1, 2, \ldots, N_2+1$. Here $r_j^{(2)}$ and $(\Phi^{(2)}_{,\lambda})_j$ are values of these fields at the collocation points. Thus, we have N_2+1 equations and N_1 equations from the first and second subdomains, respectively, which together with three transmission conditions given by (56) and (57) constitute a set of N_1+N_2+4 algebraic equations for an equal number of unknown coefficients $b_k^{(1)}(u)$ and $b_k^{(2)}(u)$. Repeating a similar procedure for the hypersurface equations (32) and (33), we obtain sets of algebraic equations for the modes $c_k^{(A)}(u)$ and $f_k^{(A)}(u)$, $A = 1, 2$.

Concerning the evolution equation (34), the vanishing of the corresponding residual equations at the collocation points in both subdomains, together with the transmission conditions, yield a set of ordinary differential equations for the coefficients $a_k^{(A)}(u)$.

The hierarchy of the field equations is preserved in the spectral representation. Specifically, once the coefficients $a_k^{(A)}(u_0)$ are initially fixed, the initial modes $b_k^{(A)}(u_0)$ are determined from the algebraic set described above. In the sequence, the remaining modes $c_k^{(A)}(u_0)$ and $f_k^{(A)}(u_0)$ can be calculated. Then, the set of ordinary differential equations determine $a_{k,u}^{(A)}(u_0)$ allowing these modes to be updated to the next time step. Repetition of this process provides the numerical solution of the field equations.

In order to evolve the self-gravitating scalar we need to specify the initial data $\Phi_0(\lambda) = \Phi(u=0,\lambda)$ that fix the initial modes $a_k^{(A)}(0)$ in both subdomains. We have chosen the three initial datasets

$$r_0(\lambda) = (1-\epsilon)\lambda + \epsilon \tanh(\lambda), \tag{61}$$

for which $\Phi_0(\lambda)$ is determined from the hypersurface equation (3),

$$\Phi_0(\lambda) = \frac{\epsilon}{1+\lambda^2} \tag{62}$$

and

$$\Phi_0(\lambda) = \frac{\epsilon}{2}(TL_{k+1}(\lambda) - TL_k(\lambda)), \tag{63}$$

determined from the Chebyshev polynomials by $TL_k(\lambda) = T_k(x = (\lambda - L_0)/(\lambda + L_0))$. Here ϵ is the parameter that plays the role of the amplitude of the initial scalar field.

VI. NUMERICAL RESULTS

We use the Bondi mass loss equation (48) to calibrate the accuracy and convergence of the code for the affine-null system. Integration of (48) gives

$$M(u) - M_0 = -\frac{1}{2}\int_{u_0}^{u} H[(H\alpha)_{,u}]^2 du, \tag{64}$$

where $M_0 = M(u_0)$ is the initial Bondi mass and $M_0(u) - M(u)$ is the mass loss evaluated at retarded time u, which equals the energy radiated in this interval described by the integral. The numerical test consists in verifying global energy conservation measured by the quantity $C(u)$ [25],

$$C(u) \equiv 1 - \frac{M(u)}{M_0} - \frac{1}{2M_0}\int_{u_0}^{u} H[(H\alpha)_{,u}]^2 du, \tag{65}$$

where $\alpha = \lim_{\lambda\to\infty}(\lambda\Phi)$ and $H = \lim_{\lambda\to\infty} r/\lambda$ [cf. (18) and (19)]. We measure the numerical deviation from the *exact* result $C(u) = 0$ by computing the maximum value of $C(u)$ for evolutions with increasing truncation order. For this test, we use the single domain Galerkin-collocation code. We evolve the initial data (61) with $\epsilon = 0.5$, corresponding to a subcritical solution, with truncation orders $N = 30, 40, 50, \ldots, 90$. The results are presented in Fig. 2. For comparison, we have included results of the same test using a similar code based upon the standard Bondi equations and coordinates. It is clear that the error for the affine-null scheme decays more rapidly.

Another important feature we have verified is the conservation of the Newman-Penrose quantity c_{NP} [cf. (37)] for both the subcritical and supercritical solutions, using the initial data (62)) with $\epsilon = 2.273172$ (subcritical) and $\epsilon = 2.273250$ (supercritical). In both cases, the log-linear plots of the relative error

$$\delta c_{NP}(u) = |c_{NP}(0) - c_{NP}(u)|/c_{NP}(0)$$

shown in Figs. 3(a) and 3(b) confirm that $c_{NP} = \text{const}$. For the supercritical solution the final Bondi mass is ≈0.0137. After black hole formation the asymptotic quantity c_{NP} is

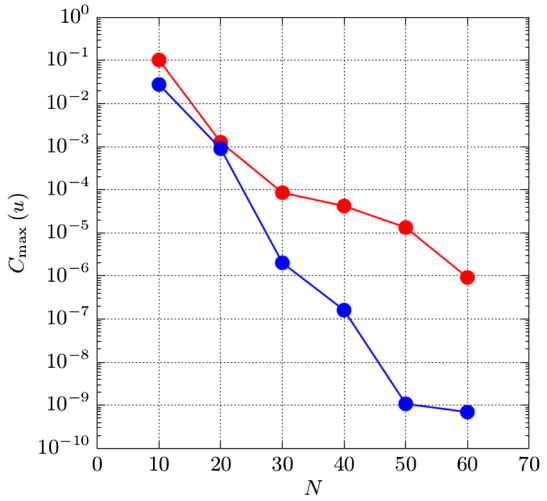

FIG. 2. Exponential decay of the maximum values of $C(u)$ for the affine-null code (blue) and the Bondi code (red). Here we have set $\epsilon = 0.5$ for the initial data (61).

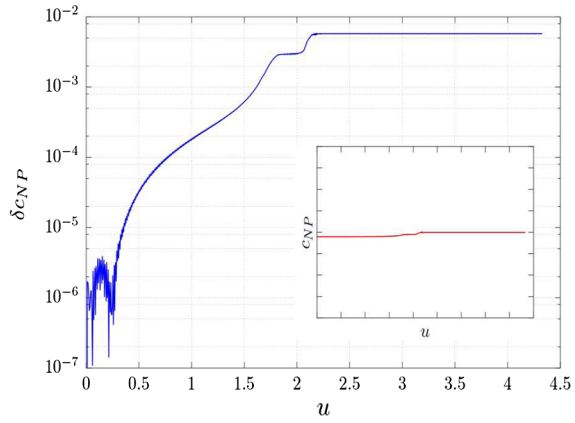

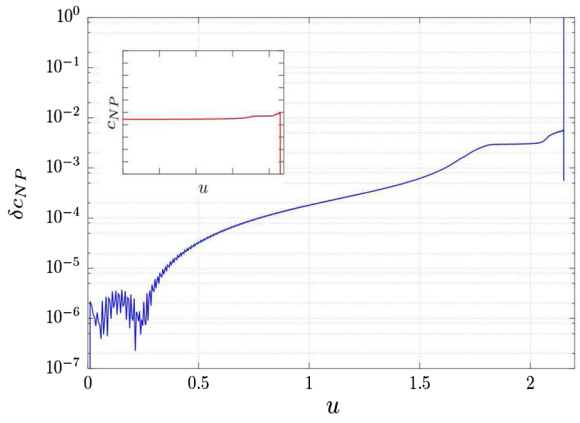

FIG. 3. The panels on the left and right, respectively, show the evolution of the relative variation δc_{NP} of the Newman-Penrose quantity for subcritical and supercritical solutions. In the corresponding insets, the conservation of c_{NP} is manifest. After black hole formation in the right panel, c_{NP} is ill defined. These solutions were generated using $\epsilon = 2.273172, 2.273250$ in the initial data (62).

not defined. In both simulations, we have used the domain decomposition algorithm with $N_1 = N_2 = 200$, $\lambda_0 = L_0 = 1.0$.

We identify the formation of a black hole in supercritical solutions by monitoring the limit $H(u) \to 0$ as $u \to u_E$ on approach to the event horizon. In terms of the global behavior of the metric function $r(u,\lambda)$, the asymptotic function $H(u)$ is computed in terms of the coefficients $b_k^{(2)}(u)$ by evaluating

$$H(u) = \lim_{\lambda\to\infty} \frac{r^{(2)}(u,\lambda)}{\lambda}. \tag{66}$$

As an illustration, we graph $H(u)$ in Fig. 4 for the subcritical (blue) and supercritical (red) solutions considered in Fig. 3. Note that due to the closeness of the initial subcritical and supercritical amplitudes, both curves almost coincide until $H(u) \to 0$ abruptly as the event horizon forms in the supercritical case. For the subcritical case, $r \to \lambda$ and $H(u) \to 1$ as the scalar field disperses. This rapid divergence in the behavior of $H(u)$ for these two cases is expected from the instability associated with the attractor underlying critical collapse.

For the supercritical solutions, the behavior of $H(u)$ provides a criterion to determine the final Bondi mass of the black hole. Recalling that $H(u)$ is positive and approaches zero as the horizon forms, we can numerically determine the moment when $H(u)$ reaches its smallest value and compute the corresponding value of the Bondi mass. In Fig. 5 we depict a typical decay of the Bondi mass together with $H(u)$ for the slightly supercritical solution generated with $\epsilon = 2.273250$ in the initial data (62). The Bondi mass decreases and reaches $M_B \approx 0.01375$. The inset shows the log-linear plot of the interval near the formation of the horizon where $H(u)$ decays rapidly to $\approx 10^{-8}$ and the Bondi mass approaches its small but nonzero final value.

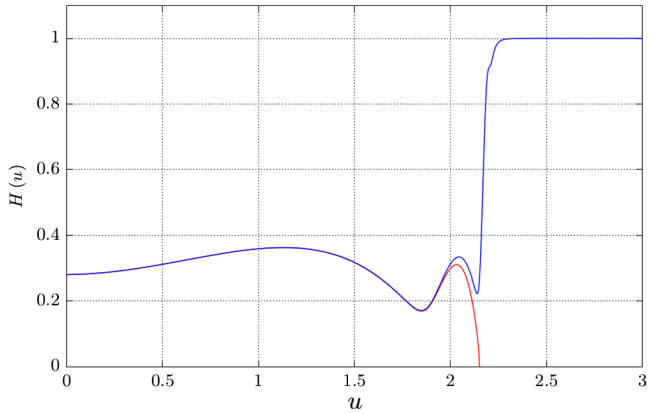

FIG. 4. Evolution of $H(u)$ for the subcritical (blue) and supercritical (red) solutions of Fig. 3. For the subcritical case, $H(u) \to 1$ as the scalar field disperses and $r \to \lambda$. For the supercritical case $H \to 0$ signaling the infinite red shift as the event horizon forms.

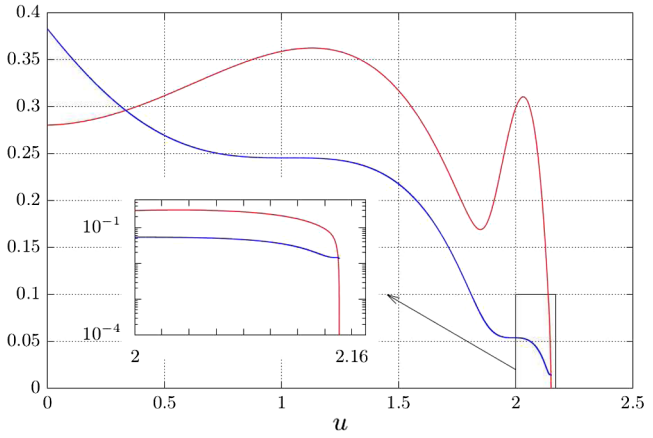

FIG. 5. The Bondi mass $M_B(u)$ (blue) and $H(u)$ (red) for the slightly supercritical solution of Fig. 3. The inset, which zooms into the interval just before horizon formation, shows that the Bondi mass approaches a small but nonzero value as $H(u)$ approaches zero.

In order to reproduce the key features of critical collapse, we have varied the initial amplitude ϵ to select the supercritical solution with the smallest final Bondi mass $M_{\rm BH}$ of the black hole using the above criterion. In this process, we find an approximate value of the critical amplitude $\epsilon_* \approx 0.7393775894$ for the initial data (61) using $N_1 = N_2 = 150$ collocation points in each domain. The numerical results plotted in Fig. 6 give an overall view of the results for $M_{\rm BH}$.

The main feature of critical collapse is the Choptuik scaling law which relates the mass M_{AH} of the apparent horizon to the critical parameter according to $M_{AH} = \bar{\kappa}(\delta\epsilon)^\gamma$, where $\delta\epsilon = \epsilon - \epsilon_*$, $\bar{\kappa}$ is a constant depending upon the initial data and γ is the critical exponent. This scaling law is

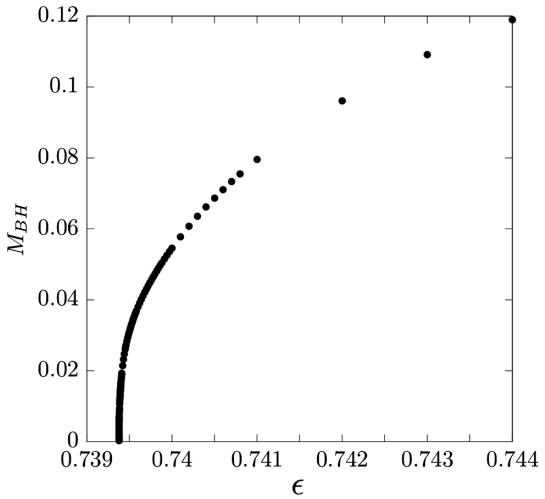

FIG. 6. Behavior of the final Bondi mass of the black hole as a function of the initial amplitude ϵ for the initial data (61).

also reflected in the final Bondi mass, as more clearly viewed in the log-log plot of Fig. 7(a) constructed with the numerical data of Fig. 6. The figure shows excellent agreement with the scaling law until $\delta\epsilon$ becomes very small on approach to the critical solution and the final Bondi mass cannot be accurately resolved. Furthermore, Gundlach [11], and Hod and Piran [26] have predicted that the original Choptuik scaling law is modified due to the discrete self-similarity (DSS) nature of the type II critical solution. They have proposed the following scaling law:

$$\ln(M_{AH}) = \gamma \ln(\delta\epsilon) + f(\delta\epsilon) + \kappa \tag{67}$$

where κ is a constant that depends on the initial data family, f is a oscillatory function with period $\varpi = \Delta/2\gamma$, and Δ is the echoing period of the DSS critical solution. Hod and Piran [26] have verified this scaling law numerically and obtained $\gamma \approx 0.37$, $\varpi \approx 4.61$ and $\Delta \approx 3.44$. Later Pürrer *et al.* [14] showed that this scaling law also closely applies to the final Bondi mass $M_{\rm BH}$ in the asymptotically flat treatment of critical collapse. They argue that this result holds because the final stage of critical collapse is dominated by the small region inside the DSS horizon.

We were able to identify the superposed oscillatory component in the numerical data for $M_{\rm BH}$ by subtracting out the $\gamma \ln(\delta\epsilon)$ term in the scaling law. The result is shown in Fig. 7(b). We obtain the critical exponent $\gamma \approx 0.37134$, the period of the oscillatory component $\varpi \approx 4.689$ and the echoing period $\Delta \approx 3.482$. Our results differ by about 1.7% from those of Pürrer *et al.* [14], which is accountable since we obtained them with only 300 grid points, 150 in each subdomain, while they used 10,000 points together with mesh refinement. Our results also show that a nonzero Newman-Penrose constant does not effect universal critical behavior.

Pürrer *et al.* [14] found another aspect of the behavior of the critical solution when described in terms of an adapted time coordinate

$$\tau_B = -\ln\left(\frac{u^* - u}{u}\right), \tag{68}$$

where u^* is the accumulation time of DSS. They showed numerically that the Bondi mass decays exponentially in τ_B, together with an oscillatory component with period $\Delta/2$. We have confirmed this feature, as illustrated in Fig. 8, for the decay of the Bondi mass in the near critical solution with $\epsilon = 0.7393775916$ for the initial data (61). In the left plot of Fig. 8, the dotted line describes $M_B \propto e^{-\tau_B}$ and the superposed oscillations have an approximate period of $\Delta/2$. The right plot zooms in on the final approach to the black hole.

We considered the formation of black holes using the initial data (62) with increased resolution by setting $N_1 = N_2 = 200$ collocation points in each subdomain and setting the map parameter $L_0 = 0.15$. We summarize the results in Fig. 9 by presenting the scaling law (left panel) and the oscillatory component (right panel). The numerical parameters are the critical exponent $\gamma \approx 0.3709$ and the oscillatory period $\varpi \approx 4.606$, resulting in an echoing period $\Delta \approx 3.417$. All these parameters agree with the results in the work of Pürrer *et al.* [14].

We repeated this numerical experiment choosing initial data (63) corresponding to $k = 5$. The approximate critical amplitude is $\epsilon_* \approx 0.458983605$ and $\gamma \approx 0.3706$. In this case, the initial oscillations in the Chebyshev polynomials lead to a large amount of ingoing radiation, some of which would cross the horizon in the supercritical case. We present a graph of the scaling law for the final Bondi mass using 400 grid points in Fig. 10. Again, as in Fig. 7,

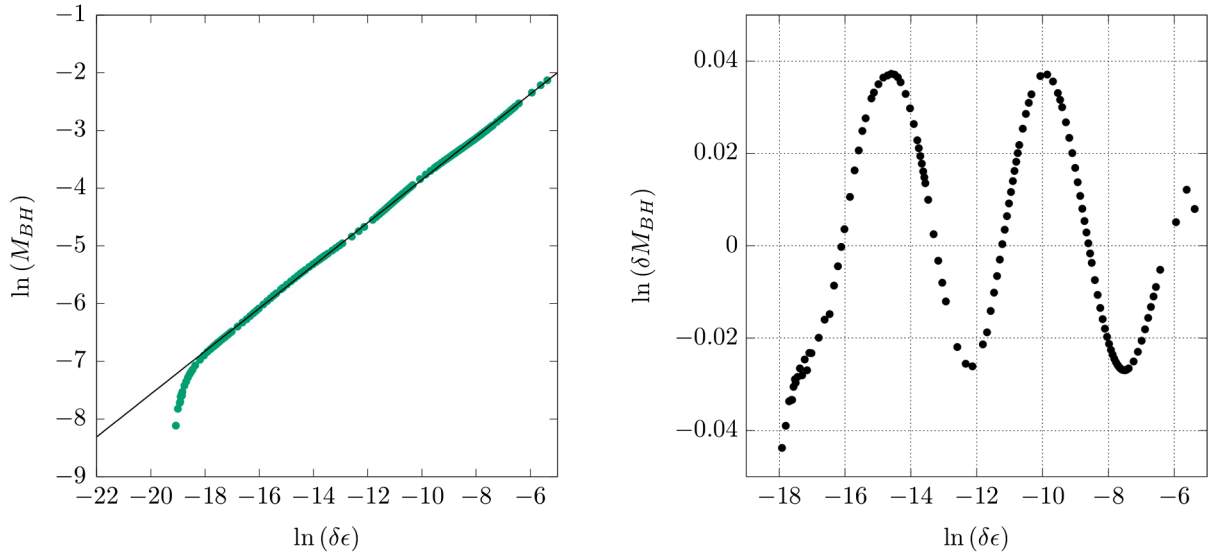

FIG. 7. Left: main scaling law $M_{\rm BH} = \bar{\kappa}(\delta\epsilon)^{\gamma}$. Right: oscillatory component $f(\delta\epsilon)$, where $\delta M_{\rm BH} = M_{\rm BH} - \bar{\kappa}(\delta\epsilon)^{\gamma}$.

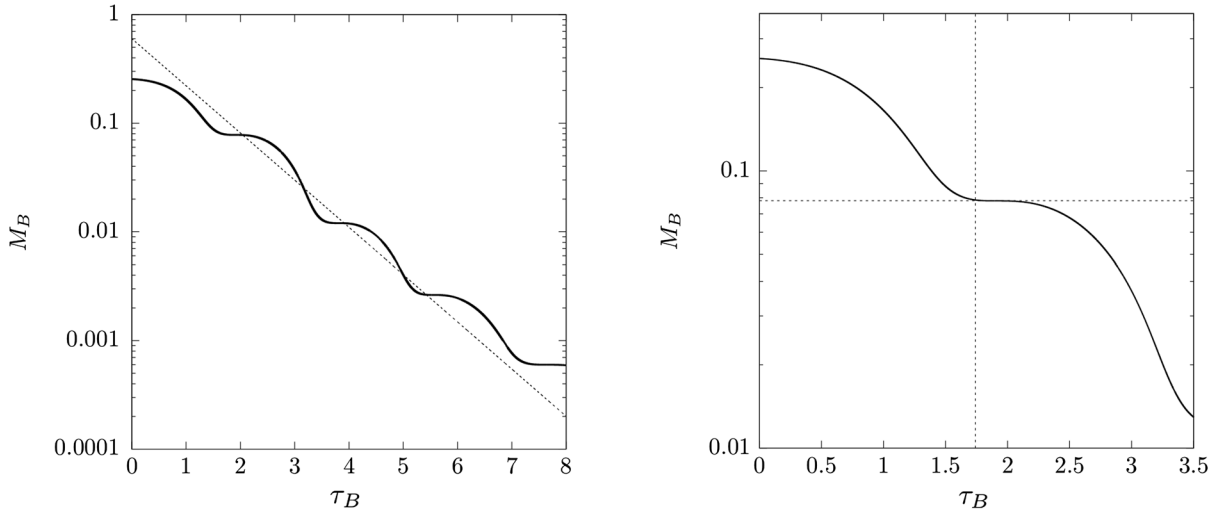

FIG. 8. Left: exponential decay of the Bondi mass represented by $M_B \propto e^{-\tau_B}$. Right: oscillation of the Bondi mass with respect to τ_B with an approximate period $\Delta/2$. Here $\epsilon_* = 0.7393775916$ for the initial data (61).

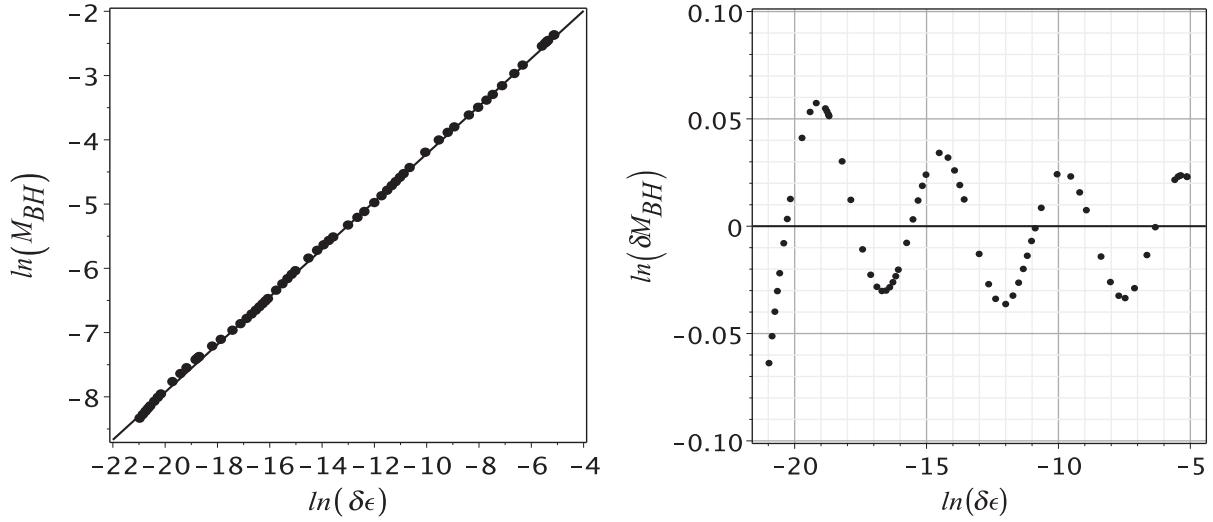

FIG. 9. Left: scaling law $M_{\rm BH} = \bar{\kappa}(\delta\epsilon)^{\gamma}$, where $\gamma \approx 0.3709$ and $\epsilon_* \approx 2.2731656922$ is the approximate critical amplitude. Right: oscillatory component $f(\delta\epsilon)$.

there is excellent agreement with the scaling law until $\delta\epsilon$ becomes very small on approach to the critical solution and the final Bondi mass cannot be accurately resolved.

This result relates to an open issue raised by Pürrer *et al.* [14]. They point out that simulations close to critical collapse prior to their work confirmed that black holes with arbitrarily small apparent horizons could be formed. But that left open the question whether black holes with arbitrarily small Bondi mass could be formed. Their numerical simulations for near critical collapse gave a small final Bondi mass but did not resolve whether a Bondi mass gap might be necessary to correct the scaling law. Numerically, this is a delicate issue since the exact critical solution is not known and, in the asymptotically flat context, might harbor a naked singularity. They conjectured that radiation crossing the outer region of the event horizon, outside the influence of the DDS behavior, might restrict the formation of black holes with arbitrarily small Bondi mass. If that were the case then the transition between subcritical and supercritical initial data would be discontinuous, i.e., it would be a transition between subcritical dispersion with zero final Bondi mass and supercritical collapse to a black hole with nonzero final Bondi mass.

This leads to an interesting confluence between the analytical and numerical results for the spherically symmetric collapse of a massless scalar field. A theorem of Christodoulou states that if the final Bondi mass is nonzero then a black hole with regular event horizon forms [20].

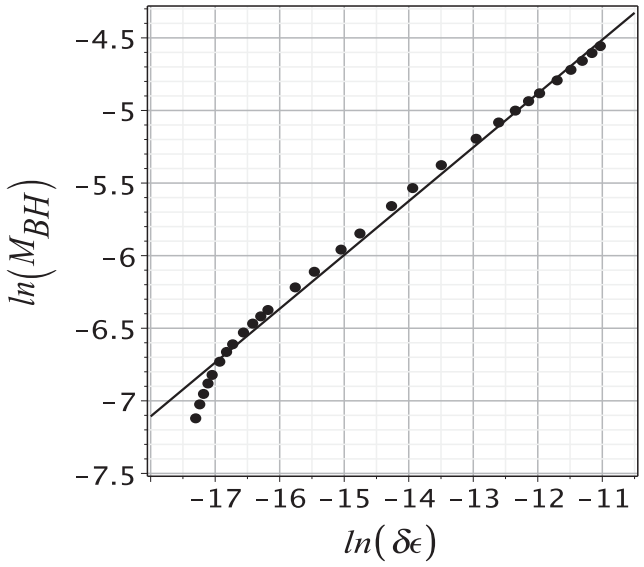

FIG. 10. Scaling law for the final Bondi mass after evolving the initial data (62) with $k = 5$. There is no evidence for a Bondi mass gap in the critical transition.

Other analytic results of Christodoulou in the asymptotically flat context, establish that naked singularities do occur in this problem, i.e., the outgoing null cone from the central world line becomes singular, although all prior outgoing null cones extend nonsingularly to $\mathcal{I}^+$, with unbounded curvature as they approach the singularity [27]. Christodoulou did not directly relate these results to the Choptuik problem but they suggest that the transition between the subcritical and supercritical cases takes place through this type of singular spacetime, as previously found in the numerical study of the nonasymptotically flat, pure DSS problem [11]. This scenario is consistent with the global numerical study by Frolov and Pen [17], although they do not explicitly compute the Bondi mass. Our results for the final Bondi mass shown in Fig. 10 show to high numerical accuracy that, even for initial data with a large amount of ingoing radiation, there is no Bondi mass gap in the transition between subcritical and supercritical evolution. In this simulation, the initial Bondi mass is approximately 0.12108 and falls between 3 and 4 orders of magnitude in the near critical evolution.

VII. DISCUSSION

In the context of spherically symmetric spacetimes with a massless scalar field, we applied a new characteristic evolution algorithm based upon an affine parameter instead of the areal coordinate of the Bondi-Sachs formulation. The advantages over the Bondi-Sachs version were discussed. In particular, the hierarchical structure of the Bondi-Sachs field equations is maintained by introducing variables which lead to unexpected quadratures and a system of equations which are regular throughout the spacetime, up to the final singularity in the case of gravitational collapse. Global regularity of the underlying equations heuristically explains the vanishing of the final scalar monopole moment, which is a corner stone of the no hair scenario for black holes. It allows a nonsingular treatment of the event horizon and black hole formation, as opposed to the Bondi-Sachs system which degenerates on the event horizon. In addition, the equations are simpler and are shown to lead to a more accurate numerical treatment.

We implemented an innovative domain decomposition evolution algorithm based upon the Galerkin-collocation method. After validating the code, we reproduced the main aspects of critical collapse such as the mass scaling law and its oscillatory component resulting from the discrete self-similarity of the critical solution. The combination of the new set of the horizon penetrating equations with spectral domain decomposition algorithm allows exhibiting these features in a grid with four hundred collocation points.

This allowed study of previously unexplored global features of the Choptuik problem for critical collapse of the scalar field. We showed that the effect of a nonvanishing Newman-Penrose constant does not affect universal critical behavior. In addition, to high numerical accuracy, our results indicate, in the context of an asymptotically flat exterior, that the final Bondi mass vanishes in the limit of critical collapse, i.e., the critical case has no Bondi mass gap. This complements the analogous result for measurements of the size of the apparent horizon for the Choptuik problem. Our study encourages the application of the affine-null system to other problems.

ACKNOWLEDGMENTS

J. C. acknowledges the financial support of the Brazilian agency Fundação Carlos Chagas Filho de Amparo à Pesquisa do Estado do Rio de Janeiro (FAPERJ). H. P. d. O. thanks Conselho Nacional de Desenvolvimento Científico e Tecnológico (CNPq) and Fundação Carlos Chagas Filho de Amparo à Pesquisa do Estado do Rio de Janeiro (FAPERJ) [Grant No. E-26/202.998/518 2016 Bolsas de Bancada de Projetos (BBP)]. J. W. was supported by NSF Grants No. PHY-1505965 and No. PHY-1806514 to the University of Pittsburgh.

[1] M. van der Burg, H. Bondi, and A. Metzner, Gravitational waves in general relativity. VII. Waves from axisymmetric isolated systems, Proc. R. Soc. A **269**, 21 (1962).

[2] R. Sachs, Gravitational waves in general relativity. VIII. Waves in asymptotically flat space-time, Proc. R. Soc. A **270**, 103 (1962).

[3] T. Mädler and J. Winicour, Bondi–Sachs formalism, Scholarpedia **11**, 33528 (2016).

[4] J. Winicour, The affine-null metric formulation of Einstein's equations, Phys. Rev. D **87**, 124027 (2013).

[5] R. A. Isaacson, J. S. Welling, and J. Winicour, Null cone computation of gravitational radiation, J. Math. Phys. (N.Y.) **24**, 1824 (1983).

[6] N. T. Bishop, R. Gómez, L. Lehner, M. Maharaj, and J. Winicour, High-powered gravitational news, Phys. Rev. D **56**, 6298 (1997).

[7] M. W. Choptuik, Universality and Scaling in Gravitational Collapse of a Massless Scalar Field, Phys. Rev. Lett. **70**, 9 (1993).

[8] A. M. Abrahams and C. R. Evans, Critical Behavior and Scaling in Vacuum Axisymmetric Gravitational Collapse, Phys. Rev. Lett. **70**, 2980 (1993).

[9] A. M. Abrahams and C. R. Evans, Universality in axisymmetric vacuum collapse, Phys. Rev. D **49**, 3998 (1994).

[10] C. Gundlach and J. M. Martín-García, Critical phenomena in gravitational collapse, Living Rev. Relativity **10**, 5 (2007).

[11] C. Gundlach, Understanding critical collapse of a scalar field, Phys. Rev. D **55**, 695 (1997).

[12] P. J. van der Walt and N. T. Bishop, Observational cosmology using characteristic numerical relativity: Characteristic formalism on null geodesics, Phys. Rev. D **85**, 044016 (2012).

[13] T. Mädler, On the affine-null metric formulation of general relativity, Phys. Rev. D **99**, 104048 (2019).

[14] M. Pürrer, S. Husa, and P. C. Aichelburg, News from critical collapse: Bondi mass, tails and quasinormal Modes, Phys. Rev. D **71**, 104005 (2005).

[15] R. S. Hamadé and J. M. Stewart, The spherically symmetric collapse of a massless scalar field, Classical Quantum Gravity **13**, 497 (1996).

[16] D. Garfinkle, Choptuik scaling in null coordinates, Phys. Rev. D **51**, 5558 (1995).

[17] A. V. Frolov and U.-L. Pen, Naked singularity in the global structure of critical collapse spacetimes, Phys. Rev. D **68**, 124024 (2003).

[18] E. T. Newman and R. Penrose, New conservation laws for zero rest-mass fields in asymptotically flat space-time, Proc. R. Soc. A **305**, 175 (1968).

[19] J. R. Cash and A. H. Karp, A variable order Runge-Kutta method for initial value problems with rapidly varying right-hand sides, ACM Trans. Math. Softw. **16**, 201 (1990).

[20] D. Christodoulou, A mathematical theory of gravitational collapse, Commun. Math. Phys. **109**, 613 (1987).

[21] C. W. Misner and D. H. Sharp, Relativistic equations for adiabatic, spherically symmetric gravitational collapse, Phys. Rev. **136**, B571 (1964).

[22] H. P. de Oliveira and E. L. Rodrigues, Numerical evolution of axisymmetric vacuum spacetimes: A code based on the Galerkin method, Classical Quantum Gravity **28**, 235011 (2011).

[23] J. P. Boyd, *Chebyshev and Fourier Spectral Methods* (Dover, New York, 2001).

[24] C. Canuto, M. Y. Hussaini, A. Quarteroni, and T. A. Zang, *Spectral Methods in Fluid Mechanics* (Spring-Verlag, Berlin, 1988).

[25] R. Gomez and J. Winicour, Asymptotics of gravitational collapse of scalar waves, J. Math Phys. (N.Y.) **33**, 1445 (1992).

[26] S. Hod and T. Piran, Fine-structure of Choptuik mass-scaling relation, Phys. Rev. D **55**, R440 (1997).

[27] D. Christodoulou, Examples of naked singularity formation in the gravitational collapse of a scalar field, Ann. Math. **140**, 607 (1994).